

1

Channel Models and Reliable Communication

Evgenii Krouk¹, Andrei Ovchinnikov¹, and Jussi Poikonen²

¹*St Petersburg State University of Aerospace Instrumentation, Russia*

²*Department of Information Technology, University of Turku, Finland*

1.1 Principles of Reliable Communication

Ideally, design, development and deployment of communication systems aims at maximally efficient utilization of available resources for transferring information reliably between a sender and a recipient. In real systems, typically some amount of unreliability is tolerated in this transfer to achieve a predefined level of consumption of limited resources. In modern communication systems, primary resources are time, space, and power and frequency bandwidth of the electromagnetic radiation used to convey information. Given such resources, systems must be designed to overcome distortions to transmitted information caused mainly by elements within the system itself, possible external communications, and the environment through which the information propagates. To achieve efficient utilization of available resources, knowledge of the mechanisms that cause interference in a given transmission scenario must be available in designing and analyzing a communication system.

In performance evaluation of wireless communication systems, significance of the communication channel is emphasized, since the degradation of a signal propagating from a transmitter to a receiver is strongly dependent on their locations relative to the external environment. Wireless mobile communication, where either the transmitter or the receiver is in motion, presents additional challenges to channel modelling, as it is necessary to account for variation in the signal distortion as a function of time for each transmitter–receiver pair. In developing and analyzing such systems, comprehensively modelling the transmitter–receiver link is a complicated task.

In the following, distortions caused by typical communication channels to transmitted signals are described. A common property of all communication channels is that the received signal contains *noise*, which fundamentally limits the rate of communication. Noise is typically modelled as a Gaussian stochastic process. The *additive white Gaussian noise (AWGN)* channel and its effects on typical digital modulation methods are presented in Section 1.2. Noise is added to transmitted signals at the receiver. Before arriving at the receiver terminal, signals are typically distorted according to various physical

characteristics of the propagation medium. These distortions attenuate the received signal, and thus increase the detrimental effect of additive noise on the reliability of communication. In Section 1.3 to 1.5 typical cases of distortion in wireless communication channels and models for the effects of such distortion on transmitted signals are presented.

1.2 AWGN

Distortions occurring in typical communication systems can be divided into multiplicative and additive components. In the following, some remarks and relevant results concerning additive distortion – also referred to simply as noise – are presented.

Additive noise is introduced to a wireless communication system both from outside sources – such as atmospheric effects, cosmic radiation and electrical devices – and from internal components of the receiver hardware, which produce thermal and shot noise [9]. Typically, additive distortion in a received signal consists of a sum of a large number of independent random components, and is modelled as additive white Gaussian noise, where the term *white* means that the noise is assumed to have a constant power spectral density. The Gaussian, or normal, distribution of noise is motivated by the central limit theorem (one of the fundamental theorems of probability theory), according to which the distribution of a sum of a large number of random variables approaches a normal distribution, given that these variables fulfill *Lyapunov's condition* (for details, see for example [10]).

In some cases, the received signal is also distorted by a channel-induced superposition of different components of the useful transmission, or by signals from other transmission systems. Such distortions are called *interference*, and differ from additive noise in that typically some source-specific statistical characteristics of interference are known. Thus interference is not in all cases best approximated as an additive white Gaussian process. Interference effects are strongly dependent on the communication systems and transmission scenarios under consideration. Later in this chapter, interference-causing effects of wireless communication channels are considered. In the following, we focus on considering the effects of additive white Gaussian noise on *complex baseband* modulation symbols. Principles of digital modulation methods and the effects of noise on the reception of various types of transmitted signals will be considered in more detail in Chapter 2; the following simple examples are meant to illustrate the concept of additive noise and its effect on digital communication.

1.2.1 Baseband Representation of AWGN

In the following examples, we consider digital data which is mapped to binary phase shift keying (BPSK), quaternary phase shift keying (QPSK/4-QAM), and 16-point quadrature amplitude modulation (16-QAM) symbols. We consider complex baseband signals, that is, for our purposes the transmitted modulation symbols corresponding to a given digital modulation scheme are represented simply as complex numbers. The constellation diagrams for these examples are illustrated in Figure 1.1. The effect of an AWGN channel is to shift these numbers in the complex plane. The receiver has to decide, based on an observed shifted complex number, the most likely transmitted symbol. This decision is performed by finding which, out of the set of known transmitted symbols, is the one with the smallest Euclidian distance to the received noisy symbol. This is a rather abstract representation of digital signals and noise, but sufficient for performing error performance analyses of different modulation schemes. For a more detailed discussion on basic modulation methods and the corresponding signal forms, see Chapter 2.

As outlined above, in complex baseband signal-space representations, the effect of additive white Gaussian noise in the receiver can be described as a complex number added to each transmitted modulation symbol value. The real and imaginary parts of these complex numbers are independent and identically distributed Gaussian random variables with zero mean and variance equal to $\sigma_N^2 = \bar{P}_N/2$, where \bar{P}_N denotes the total average power of the complex noise process (that is, the power of the noise

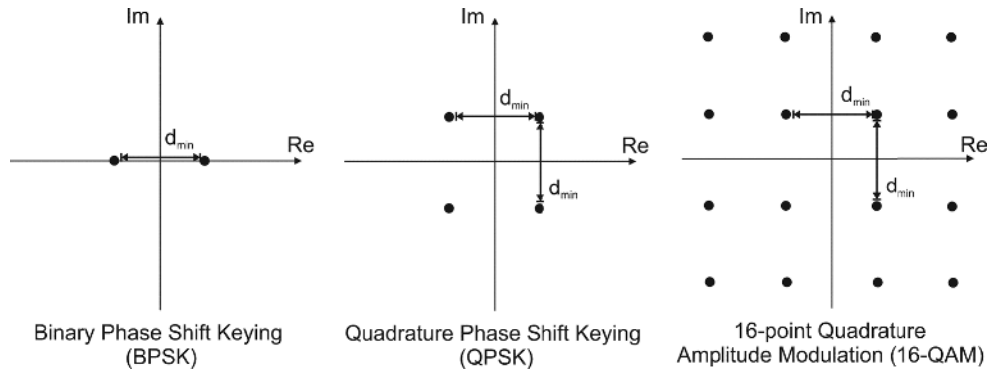


Figure 1.1 Example of signal constellations corresponding to BPSK, QPSK, and 16-QAM modulation schemes

is evenly distributed into the two signalling dimensions). In the following, the orthogonal components of the noise process are denoted by a common notation $X_N \sim N(0, \bar{P}_N/2)$.

If the absolute value of either the real or the imaginary noise component is larger than half of the Euclidian distance d between adjacent modulation symbols, a transmitted symbol may be erroneously decoded into any symbol within a complex half-plane, as illustrated in the QPSK example of Figure 1.2. The probability of one of the independent and identically distributed noise components having such values can be written as:

$$P(X_N > d/2) = \int_{d/2}^{\infty} \frac{1}{\sqrt{\pi \bar{P}_N}} \exp\left(-\frac{x^2}{\bar{P}_N}\right) dx = 1 - \int_{-\infty}^{\frac{d}{\sqrt{2\bar{P}_N}}} \frac{1}{\sqrt{2\pi}} \exp\left(-\frac{x^2}{2}\right) dx \quad (1.1)$$

where the final expression is given in terms of the cumulative distribution function of a normalized Gaussian random variable. Error probabilities are usually specified in this form, since the Q -function $Q(\alpha) = 1 - \int_{-\infty}^{\alpha} \frac{1}{\sqrt{2\pi}} \exp(-\frac{x^2}{2})$ is widely tabulated in mathematical reference books, and easily calculated with programs such as Matlab. The expression (1.1) gives directly the probability of error for BPSK, and can be used to calculate the average probability of error for larger QAM constellations. In Figure 1.3, the principle of calculating the symbol error probability of QPSK using (1.1) is illustrated. The same principle is applied in Figure 1.4 to 16-QAM, where several different error cases have to be considered, and averaged to obtain the total probability of symbol error.

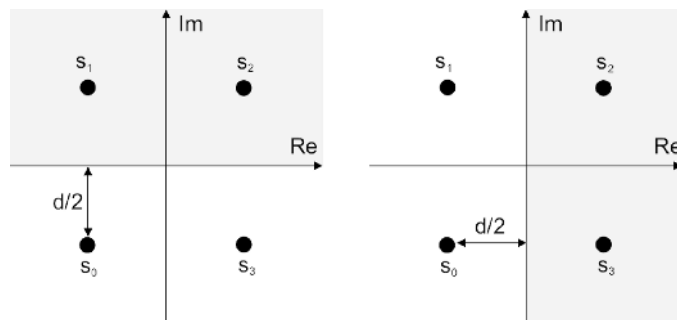


Figure 1.2 The effect of noise on a QPSK signal constellation. Left: imaginary component of noise is larger than $d/2$ – transmitted symbols s_0 and s_3 will be erroneously decoded either as s_1 or s_2 . Right: real component of noise is larger than $d/2$ – transmitted symbols s_0 and s_1 will be erroneously decoded either as s_2 or s_3

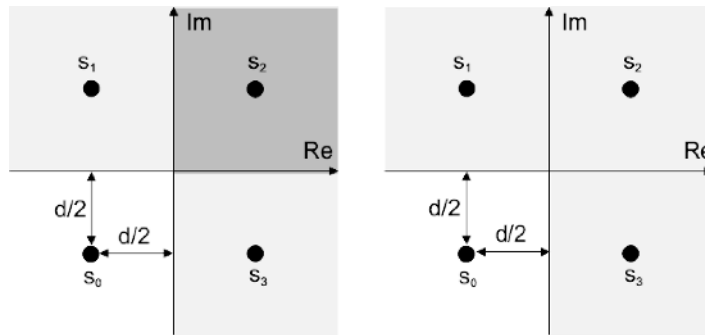


Figure 1.3 Principle of calculating the probability of symbol error for a QPSK signal constellation, assuming s_0 is transmitted. Left: $2P(X_N > d/2)$ includes twice the probability of receiving a value in the diagonally opposite quadrant. Right $2P(X_N > d/2) - P(X_N > d/2)^2$ is the correct probability of symbol error

In the preceding examples, the error probabilities are calculated in terms of the minimum distance of the constellations and the average noise power. However, it is more convenient to consider error probabilities in terms of the ratio of average signal and noise powers. For any uniform QAM constellation, the distance between any pair of neighbouring symbols (that is, the minimum distance) is easily obtained as a function of the average transmitted signal power \bar{P}_S – which is calculated as the average over the squared absolute values of the complex-valued constellation points – as:

$$d = \begin{cases} 2\sqrt{\bar{P}_S} & \text{(BPSK)} \\ 2\sqrt{\bar{P}_S/2} & \text{(QPSK)} \\ 2\sqrt{\bar{P}_S/10} & \text{(16-QAM)} \end{cases}$$

The average symbol error probability for each of the cases above is now obtained by calculating averages over demodulation error probabilities for the signal sets as a function of the average signal-to-noise ratio, given by $\bar{P}_S/\bar{P}_N \triangleq \lambda$. Using the equations given above, the average symbol error probabilities are

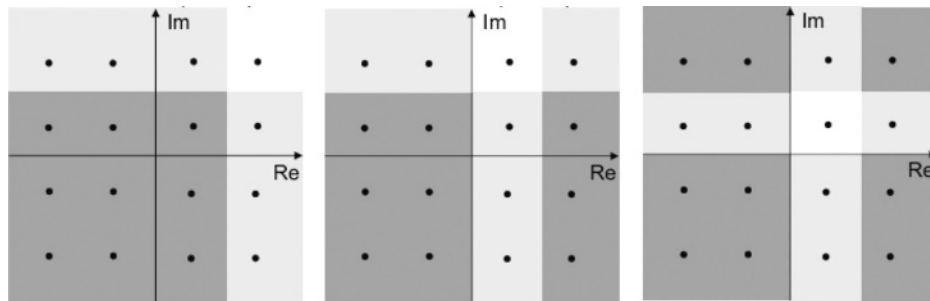


Figure 1.4 Principle of calculating the probability of symbol error for a 16-QAM signal constellation. Left: for the four corner symbols, the probability of symbol error is $2P(X_N > d/2) - P(X_N > d/2)^2$. Center: for the eight outer symbols, $3P(X_N > d/2) - 2P(X_N > d/2)^2$. Right: for the middle symbols, $4P(X_N > d/2) - 4P(X_N > d/2)^2$. The total probability of symbol error is the weighted average of these probabilities

obtained, following the principle outlined in the examples of Figures 1.3 and 1.4, as:

$$p_s(\lambda) = \begin{cases} Q(\sqrt{2\lambda}) & \text{(BPSK)} \\ 2Q(\sqrt{\lambda}) - Q(\sqrt{\lambda})^2 & \text{(QPSK)} \\ 3Q(\sqrt{\lambda/5}) - \frac{9}{4}Q(\sqrt{\lambda/5})^2 & \text{(16-QAM)} \end{cases}$$

1.2.2 From Sample SNR to E_b/N_0

Assume the transmitted symbols are mapped to rectangular baseband signal pulses of duration T_{sym} , sampled with frequency f_{samp} , with complex envelopes corresponding to the constellation points of the signal-space representation used above. These rectangular pulses are then modulated by a given carrier frequency, transmitted through a noisy channel, downconverted in a receiver and passed to a matched filter or correlator for signal detection.

Figure 1.5 shows an example of two BPSK symbols transmitted and received as described above. In this example, the signal-to-noise ratio per sample is defined as $SNR = A^2/\sigma_n^2$, where σ_n^2 is the sample variance of the real-valued noise process. It can be seen that, based on any individual sample of the received signals, the probability of error is quite large. However, calculating the averages (plotted with dashed lines in Figure 1.5) of the signals over their entire durations (0.1 s, containing 100 samples) gives values for the signal envelopes that are very close to the correct values -1 and 1 , thus reducing the effect of the added noise considerably. It is clear that in this case, the sample SNR is no longer enough to determine the probability of error at the receiver. The relevant question is how should the sample SNR be scaled to obtain the correct error probability? We study this using BPSK as an example.

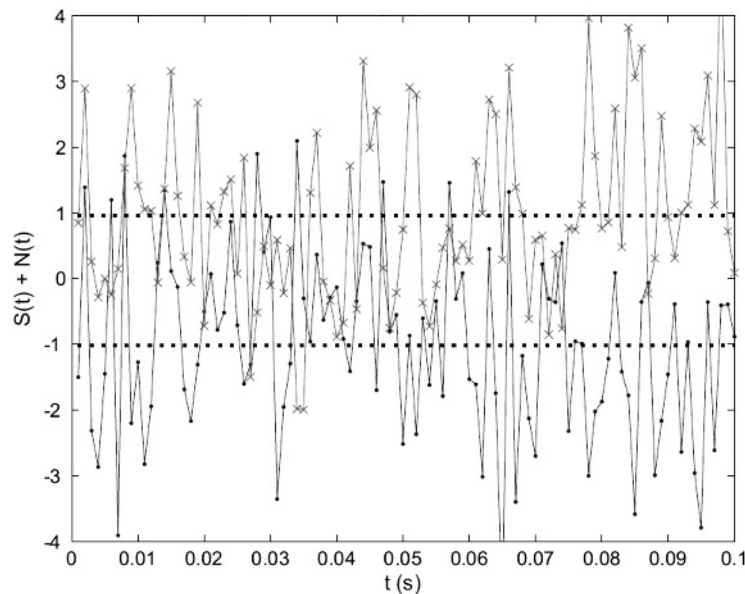


Figure 1.5 Two noisy signal envelopes and their averages. For this example, $T_{\text{sym}} = 0.1$ s, $f_{\text{samp}} = 1000$ Hz, $A_1 = -A_0 = 1$, $E_b/N_0 = 15$ dB \leftrightarrow SNR = -5 dB

As above, the probability of symbol (bit) error based on the signal-space representation for BPSK over an AWGN channel is:

$$P_e = P(N < -A_1) = \int_{-\infty}^{-A_1} \frac{1}{\sigma_n \sqrt{2\pi}} \exp\left(-\frac{x^2}{2\sigma_n^2}\right) dx$$

where N is a normally distributed random variable with standard deviation σ_n and zero mean, and it is assumed (without loss of generality) that the signal amplitude $A_1 > 0$ (corresponding to a 1 being sent). This can be thought of as transmitting a single sample of the signal envelope. Sampling a received signal envelope $S(t) + N(t)$ at k points produces a sequence of samples $S(i \cdot T_{\text{sampl}}) + N(i \cdot T_{\text{sampl}})$, where $T_{\text{sampl}} = 1/f_{\text{sampl}}$, and $i = 1 \dots k$. A correlator receiver for BPSK may use the following test statistic to decide whether a 1 was most likely to be transmitted:

$$Z = A_1 \left(\sum_{i=1}^k (S(i \cdot T_{\text{sampl}}) + N(i \cdot T_{\text{sampl}})) \right) = \sum_{i=1}^k (A_1 S(i \cdot T_{\text{sampl}})) + \sum_{i=1}^k (A_1 N(i \cdot T_{\text{sampl}}))$$

Assuming that a 1 was indeed sent, a false decision will be made if:

$$A_1 \sum_{i=1}^k N(i \cdot T_{\text{sampl}}) < -k \cdot A_1^2 \Leftrightarrow \frac{1}{k} \sum_{i=1}^k N(i \cdot T_{\text{sampl}}) < -A_1$$

or

$$\bar{N} < -A_1$$

denoting the sample mean of the noise as \bar{N} . We note that the expression is the same as for the single sample case, only with the normal random variable replaced by the sample mean of k samples from a normal distribution. Basic results of statistics state that this sample mean is also normally distributed, in this case with mean zero and standard deviation $\sigma_{\bar{N}} = \sigma_n / \sqrt{k}$. We thus find that the error probability in this example is determined by the ratio $k \cdot (\sigma_s^2 / \sigma_n^2)$, or k times the sample SNR.

It should be noted that although we used BPSK as an example to simplify the relevant expressions, the above result is not restricted only to BPSK. In fact, the obtained expression $k \cdot (\sigma_s^2 / \sigma_n^2)$ is generally used in a form derived as follows:

$$k \cdot \frac{\sigma_s^2}{\sigma_n^2} = \frac{T_{\text{symp}}}{T_{\text{sampl}}} \cdot \frac{\bar{P}_S}{\bar{P}_N} = \frac{\bar{P}_S \cdot T_{\text{symp}}}{(1/f_{\text{sampl}}) \cdot N_0 B_n} = \frac{E_S}{N_0}$$

In the above, N_0 is the noise power spectral density and B_n is the noise bandwidth. Note that the signal energy $E_S = \bar{P}_S \cdot T_{\text{symp}}$, and that $B_n = f_{\text{sampl}}$ (this is based on the Shannon-Nyquist sampling theorem applied for complex samples). Note also that here it is implicitly assumed that the signal bandwidth corresponds to the Nyquist frequency; if the signal is oversampled, care should be taken in performance analysis to include only the noise bandwidth which overlaps with the spectrum of the signal. Finally, the ratio of energy per bit to noise power spectral density E_b/N_0 , very commonly used as a measure for signal quality, is obtained as:

$$\frac{E_b}{N_0} = \frac{1}{n_b} \frac{E_s}{N_0}$$

where n_b is the number of bits per transmitted symbol.

1.3 Fading Processes in Wireless Communication Channels

Additive noise is present in all communication systems. It is a fundamental result of information theory that the ratio of signal and noise powers at the receiver determines the capacity, or maximum

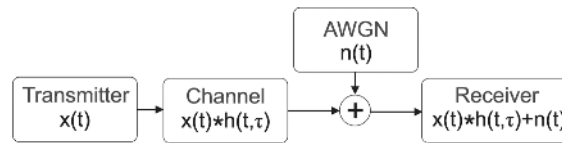


Figure 1.6 System model for transmitting information through a channel with additive white Gaussian noise

achievable rate of error-free transmission of information, of a channel. Generally, multiplicative effects of a communication channel, or *fading*, can be represented as a convolution of the transmitted signal with the *channel impulse response*, as illustrated in Figure 1.6. A general effect of fading is to reduce the signal power arriving at the receiver. Since the noise power at the receiver is independent of the useful signal, and the noise component does not experience fading, a fading channel generally reduces the ratio of the signal power to the noise power at the receiver, thus also reducing the transmission capacity.

The distortion, or noise, caused by a communication channel to the transmitted signal can be divided into multiplicative and additive components; the latter was considered above. Multiplicative noise, or fading, can be defined as the relative difference between the powers contained in corresponding sections of the transmitted and received signals. Factors that typically contribute to the fading in wireless communication systems are the transmitter and receiver antenna and analog front-end characteristics, absorption of the signal power by the propagation media, and reflection, refraction, scattering and diffraction caused by obstacles in the propagation path. The receiver experiences the combined effect of all these physical factors, which vary according to the positions of the receiver and transmitter within the propagation environment. It should be noted that it is generally possible to describe the effects of a communication channel entirely by its impulse response as illustrated in Figure 1.6. However, it is typical that estimation of the average power conveyed by a transmission channel is performed separately from the modelling of the channel's impulse response, which is then power-normalized. We also apply this principle in the following discussion on *fading processes* in wireless channels.

Fading in wireless channels is in literature typically characterized as a concatenation or superposition of several types of fading processes. These processes are often classified using the qualitative terms *path loss*, *shadowing*, and *multipath fading*, which is also often referred to as *fast fading*. However, these fading processes cannot in general be considered fully independent of each other, and indeed in many references (for example in [1],[12]) path loss and shadowing are not considered as separate processes. Justification for this will be subsequently considered in more detail. In the following, fading is primarily classified according to the typical variation from the mean attenuation over a spatial region of given magnitude. The terms large-scale, medium-scale, and small-scale fading are thus used.

Small-scale fading corresponds directly to multipath fading, and involves signal power variations of magnitude up to 40 dB on a spatial scale of a half-wavelength (for example 50 cm at 300 MHz). Averaging the total fading in the receiver over a spatial interval significantly larger than a half-wavelength provides information on the medium-scale fading, or shadowing. Over spatial intervals of magnitude hundreds of meters, medium-scale fading involves signal power variations up to magnitude 20 dB. Again, averaging the total fading over a spatial interval of several hundred meters provides an estimate for the large-scale fading, which may vary up to 150 dB over the considered coverage area. [9] These denominations do not suggest a different origin or effect for the fading types, but rather signify that typically different variation around the mean attenuation is observed at different spatial scales, or observation windows.

1.3.1 Large-Scale Fading (Path Loss)

Large-scale fading, or path loss, is commonly modelled for signals at a given carrier frequency as a deterministic function of the distance between the transmitter and receiver, and is affected by several

parameters such as antenna gains and properties of the propagation environment between the transmitter and receiver. Main physical factors that contribute to large-scale fading are free-space loss, or the dispersion of the transmitted signal power into surrounding space, plane earth loss, and absorption of the signal power by the propagation medium.

Free-space loss corresponds to dispersion of transmitted signal power into the space surrounding the transmitter antenna. The most simple free-space loss estimation is obtained by assuming that signals are transmitted omnidirectionally, that is, power is radiated equally to all directions, and there are no obstacles within or around the transmission area, which would affect the propagation of electromagnetic signals. With such assumptions, the *power density* at a distance d meters from the transmitter can be written as:

$$p_R = \frac{P_T}{4\pi d^2} \text{ (watts/m}^2\text{)}$$

where P_T is the total transmitted signal power. This expression is obtained simply by dividing the transmitted power over the surface area of a sphere surrounding the transmitter antenna.

The assumptions specified above are not practical in most communication scenarios. Ignoring for now the likely presence of obstacles around the transmitter and receiver, the free-space loss defined above can be modified into a more realistic expression by taking into account the antenna characteristics of the transmitter and receiver. Specifically, the actual received power depends on the *effective aperture area* of the receiver antenna, which can be written as:

$$A_R = \frac{\lambda^2 G_R}{4\pi} \text{ (m}^2\text{)}$$

where λ is the wavelength of the transmitted signal and G_R is the receiver *antenna gain*, which is affected by the directivity of the antenna – specifically the antenna radiation patterns in the direction of the arriving signal. It should be noted that the above expression means that the received power decreases along with an increase in the carrier frequency. Finally, taking into account the transmitter antenna gain factor G_T , the received power after free-space loss can be written as:

$$P_R = G_T p_R A_R = \frac{P_T G_T G_R \lambda^2}{(4\pi d)^2} \text{ (W)}$$

Note that in the above, the variables are assumed to be given in the linear scale, that is, not in decibels. Figure 1.7 shows examples of the received power as a function of distance from the transmitted antenna for different carrier frequencies, with the antenna gains and transmitted signal power normalized to unity. Formally, an expression for the path loss P_L , that is, attenuation of the transmitted signal, is obtained from the above in decibels as:

$$P_{L,dB} = 10 \log_{10} \frac{P_T}{P_R} = 10 \log_{10} \frac{(4\pi d)^2}{G_T G_R \lambda^2} = 20 \log_{10}(4\pi d) - 10 \log_{10}(G_T) - 10 \log_{10}(G_R) - 20 \log_{10}(\lambda)$$

Real signals do not follow the simple free-space attenuation model partly due to the presence of the ground plane close to the transmitter and receiver. This causes so called plane earth loss, where signal components reflected from the ground plane destructively interfere with the received useful signal. The amount of plane earth loss depends on the distance and heights of the transmitter and receiver antennas. Another significant cause for attenuation is the absorption of signal power by atmospheric gases and hydrometeors (such as clouds, rain, snow etc.).

In addition to these factors, large-scale fading is typically defined to include the average of the shadowing and multipath fading effects. Thus the type of propagation environment must be taken into account in the total power loss. This has been done for example in the widely used Okumura-Hata [13],[14] and COST 231 [15] models by approximating the parameters for the propagation loss for specific environments and transmission setups from sets of field measurements [1]. As an example, the

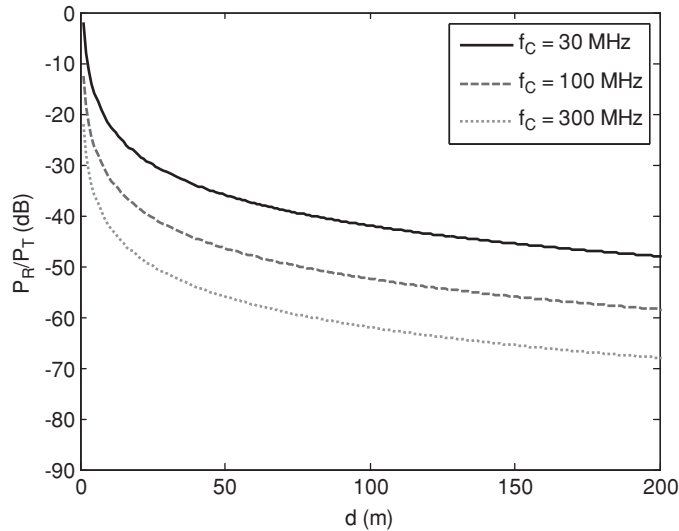


Figure 1.7 Examples of free-space loss for different carrier frequencies f_C , with the antenna gains and transmitted power normalized to 1

Hata model, which is based on the empirical work of Okumura, gives the following expression for path loss in urban areas (in dB):

$$P_{L,dB}(d) = 69.55 + 26.16 \log_{10}(f_C) - 13.82 \log_{10}(h_T) - a(h_R) + [44.9 - 6.55 \log_{10}(h_T)] \log_{10}(d)$$

where f_C is again the carrier frequency, h_T and h_R are the heights of the transmitter and receiver antennas, respectively, and $a(h_R)$ is a correction factor, which is specified according to the size of the considered reception area. For large urban areas with the carrier frequencies of magnitude $f_C > 300$ MHz, this correction factor is given as:

$$a(h_R) = 3.2(\log_{10}(11.75h_R))^2 - 4.97$$

For other propagation scenarios, such as suburban and various rural areas, correction terms for the path loss expression given above are specified.

The Hata model is considered to be valid roughly in the carrier frequency range 150—1500 MHz and for distances $d > 1$ km, which means that it is not generally valid for example for modelling modern cellular systems with high carrier frequencies and small cell sizes [19]. In the European COST 231 cooperation, an extension to the Hata model was specified, where the carrier frequency is restricted between 1.5 and 2 GHz, the transmitter antenna height between 30 to 200 m, the receiver antenna between 1 and 10 m, and the transmission distance between 1 and 20 km. With these limitations, the path loss for an urban scenario according to the COST 231 extension to the Hata model is obtained from [15] as:

$$P_{L,dB}(d) = 46.3 + 33.9 \log_{10}(f_C) - 13.82 \log_{10}(h_T) - a(h_R) + [44.9 - 6.55 \log_{10}(h_T)] \log_{10}(d) + C$$

where $a(h_R)$ is as in the Hata model, and C is 0 dB for medium-size urban areas and suburbs, and 3 dB for metropolitan areas.

The *empirical path loss models* outlined above are determined by averaging the results of large sets of measurements performed in propagation environments with specific characteristics. Similar path loss models can be obtained using analytic methods by assuming a statistical terrain description,

where obstacles of suitable geometry are distributed randomly in the propagation environment, and by calculating the average propagation loss based on such approximations. For example, [11] contains a detailed description of deriving functions for path loss in various land environments using analytic methods. The physical mechanisms that cause the environment-specific propagation loss are the same for large-scale fading as for medium-scale fading, and are considered in more detail shortly.

Deterministic large-scale fading models – where estimations of the path loss are obtained as functions of the propagation distance – are useful in applications where it is sufficient to have rough estimates on the average attenuation of signal power over a large transmission area, or it is impractical to approximate signal attenuation in more detail. These models are typically used for example in radio resource management and planning of large wireless networks. It should be noted that expressions for large-scale fading can be obtained for generic environments using statistical methods as outlined above or for specific transmission sites by averaging over a site-specific approximation of medium-scale fading. However, this is typically a computationally involved task, as described in the following.

1.3.2 Medium-Scale Fading (Shadowing)

As with large-scale fading, methods for modelling medium-scale fading can typically be categorized as statistical or site-specific. In the statistical approach, the fading is typically assumed – based on empirical data – to follow a lognormal distribution. The mean for this distribution can be obtained for a given carrier frequency and distance from the transmitter using expressions for large-scale fading as outlined in the previous subsection. The standard deviation and autocorrelation of the lognormal distribution are model parameters, which must be selected according to the propagation environment. This standard deviation is known as the location variability, and it determines the range of fluctuation of the signal field strength around the mean value. Its value increases with frequency, and is also dependent on the propagation scenario – for example, the standard deviation is typically larger in suburban areas than in open areas. The standard deviation is typically in the range of 5 to 12 dB. Spatial correlation of shadowing is usually modelled using a first-order exponential model [20]:

$$\rho(d) = e^{-d/d_{corr}}$$

where d_{corr} is the distance over which the correlation is reduced by e^{-1} . This distance is typically of the same order as the sizes of blocking objects or object clusters within the transmission area.

An intuitive justification for the applicability of a lognormal model for medium-scale, or shadow fading, can be obtained by considering the total attenuation of the signal components arriving at the receiver in an environment with a large number of surrounding obstacles. Typically the signal components arriving at the receiver have passed through a number of obstacles of random dimensions, each attenuating the signal power by some multiplicative factor. The product of these fading factors contributes to the total power attenuation. In the logarithmic scale, the product of several fading components is represented as the sum of their logarithms, and again according to the central limit theorem the distribution of this sum approaches a normal distribution. Figure 1.8 shows examples of log-normal medium-scale fading for standard deviation 10 dB, and correlation distances 20 and 50 meters.

If site-specific data on the terrain profile and obstructions along the propagation path from the transmitter to the receiver are available, an approximation for medium-scale fading can be calculated as summarized in [9]:

1. Locate the positions and heights of the antennas.
2. Construct the great circle – or geodesic – path between the antennas. This represents the shortest distance between the two terminals measured across the Earth's surface.
3. Derive the terrain path profile. These are readily obtained from digital terrain maps, but it is of course also possible to use traditional contour profile maps.

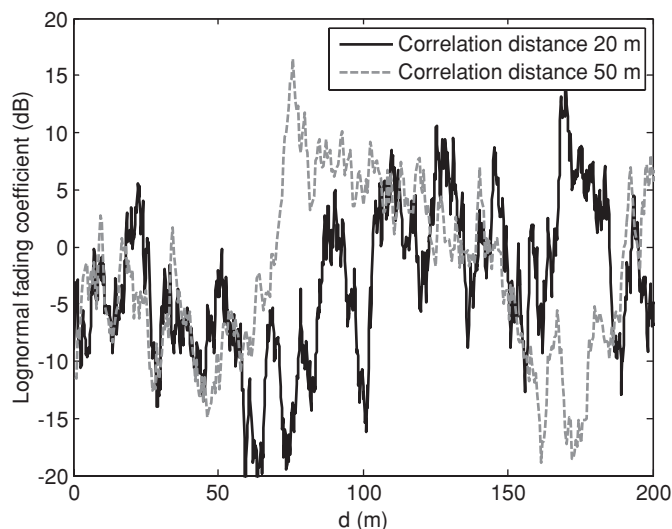


Figure 1.8 Examples of lognormal medium-scale fading processes with standard deviation 10 dB, and correlation distances 20 and 50 meters

4. Uplift the terrain profile by representative heights for any known buildings along the path.
5. Select a value for the effective Earth radius factor appropriate to the percentage of time being designed for; modify the path profile by this value. The effective Earth radius factor is a constant used to increase the effective radius of the Earth as seen by the propagating signal. This is due to tropospheric refraction, which makes the propagation paths curve slightly towards the ground. Since the atmospheric refractivity varies with pressure, temperature and water vapour pressure of the atmosphere, the correct effective Earth radius factor will vary according to location and time.
6. Calculate the free-space loss for the path.
7. If any obstructions exist within 0.6 times the first Fresnel zone of the propagation path, calculate diffraction over these obstructions and account for the excess loss in the fading. The Fresnel zones can be thought of as containing the main propagating energy in the wave; obstructions occupying less than 0.6 times the first Fresnel zone lead to an approximately 0 dB loss of signal power.
8. Compute the path length which passes through trees and add the corresponding extra loss.

Detailed descriptions for each of the steps above are given in [9]. It should be noted that the approach outlined above accounts only for obstructions along the direct propagation path between the transmitter and receiver. Considering propagation paths corresponding to reflections from objects not along the direct path leads to small-scale fading models, considered in the following sections.

1.3.3 Small-Scale Fading (Multipath Propagation)

Small-scale fading is caused by the interference between several reflected, diffracted or scattered signals arriving at the receiver. This effect is commonly called *multipath propagation*. Since the reflected propagation paths may be of different lengths, corresponding to different arrival times for variously faded copies of the transmitted signal at the receiver, the effect of small-scale fading is in the digital domain similar to a finite impulse response (FIR) filter with complex-valued coefficients between the transmitter and receiver. Thus, depending on the path delay profile of the channel, small-scale fading

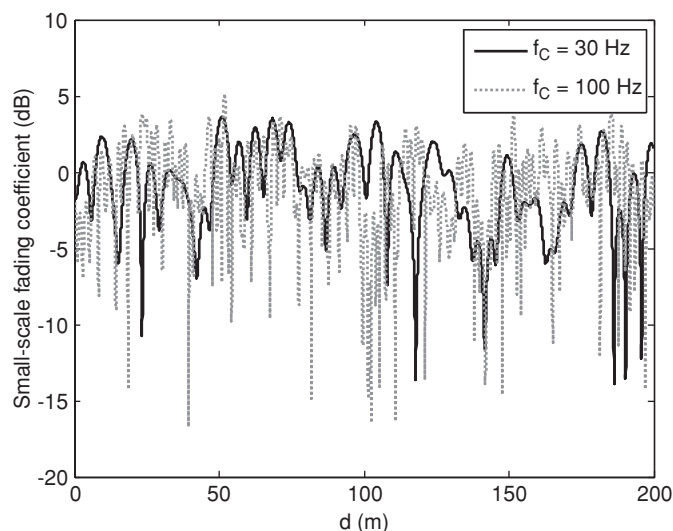


Figure 1.9 Examples of small-scale Rayleigh fading processes with normalized average power, and carrier frequencies of 30 and 100 Hz

may vary rapidly not only in the temporal and spatial domains, but also in the frequency domain. The rate of spatial variation of small-scale power attenuation is generally dependent on the carrier frequency of the transmitted signal. Figure 1.9 shows examples of small-scale fading for carrier frequencies 30 and 100 Hz. Figure 1.10 shows an example of the combined effects of large- medium- and small-scale fading.

Again, small-scale fading models can be divided into statistical and site-specific approaches. Site-specific models typically apply ray-tracing methods, where detailed three-dimensional models of the propagation environment are used to calculate propagation paths between the transmitter and receiver. Such techniques were originally developed for indoor environments, but have also been extended to dense urban outdoor areas [1]. Especially for modelling unconfined outdoor environments, ray-tracing models require large amounts of data and are computationally demanding. In the rest of this chapter we focus on statistical models for multipath propagation.

The causes of multipath propagation may be different in different channels. For example, it may be caused by reflections from buildings, objects or the ground surface in wireless communication channels, the reflection from walls and objects in wireless local area networks, reflections from the ionosphere in high-frequency radio transmission, and so on. Multipath propagation may be schematically described as in Figure 1.11, and mechanisms causing it are listed in Table 1.1 [21],[22]. As can be seen from Table 1.1, fading and propagation delay dispersion may arise even during wired transmission.

Small-scale fading is caused by the interference of multiple signals with random relative phases. Such interference causes random variation of the amplitude of the received signal. This increases the error probability in the system, since it reduces the signal-to-noise ratio. Dispersion of the delays of signal components arriving at a receiver is caused by the difference in the lengths of different propagation paths. If the delay difference is comparable with the symbol period, then the delayed responses from one signal may impose on the next signal, causing *intersymbol interference (ISI)* and frequency-selective fading.

One of the most common models for delay-dispersive wireless propagation channels is the representation of the channel as a *linear filter*. The channel is described by a time-varying impulse response $h(\tau, t)$. Applying the Fourier transform to $h(\tau, t)$ by the variable τ gives the *time-varying frequency response*

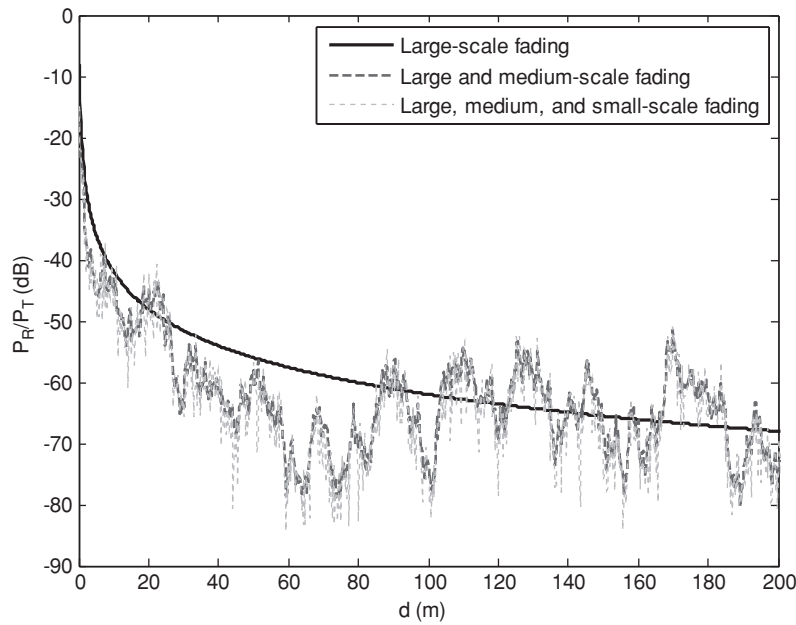


Figure 1.10 Combined effects of the three considered fading processes (large/medium/small-scale). The normalized received power is shown for carrier frequency 300 Hz, transmitted power and antenna gains set to unity, standard deviation of lognormal shadowing 10 dB with correlation distance 20 m, and average power of Rayleigh-distributed small-scale fading set to unity

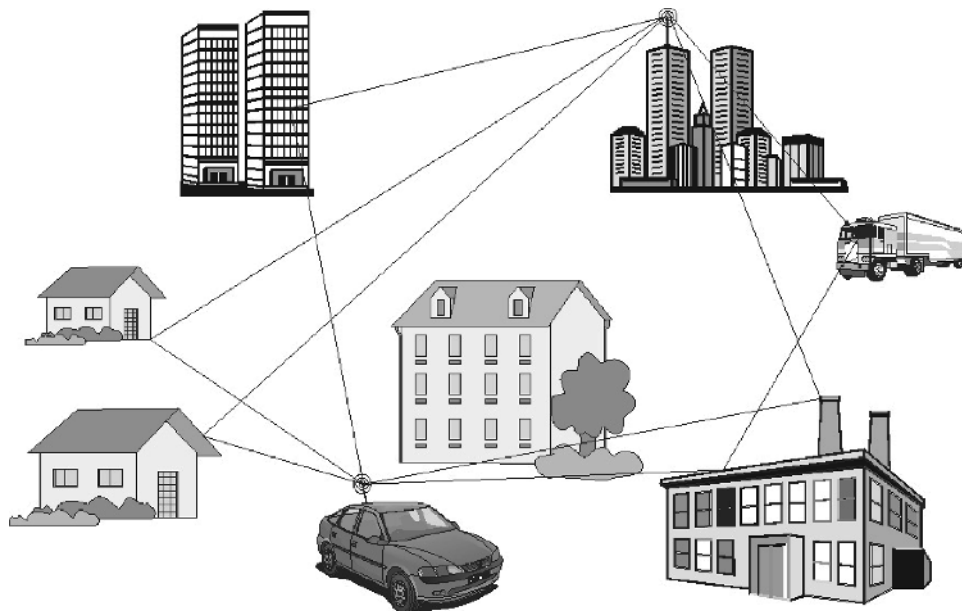


Figure 1.11 Multi-level spreading

Table 1.1 Multipath mechanisms

	System	Multipath mechanism
1	HF radio	Reflection from multiple ionospheric layers
2	Mobile and personal radio	Reflection and scattering from buildings, terrain, etc.
3	Microwave point-to-point links	Atmospheric refraction and reflection
4	Atmospheric refraction and reflection	Ground and building reflection
5	Radio LAN/indoor radio	Reflection from walls and building structure
6	Diffuse infra-red	Reflection from walls
7	Multimode optical fibre	Multimode propagation
8	Telephone/cable network	Reflections from terminations

$H(f, t)$, while the Fourier transform of $h(\tau, t)$ by the variable t gives the *scattering function* $S(\tau, \nu)$, which determines the Doppler spectrum of received signal as a function of the delay. The mean squared amplitudes of the channel impulse response define the *power delay profile* of the channel. An example of such a profile is shown in Figure 1.12. In the following section we consider in more detail this statistical model for multipath propagation outlined above.

1.4 Modelling Frequency-Nonselective Fading

1.4.1 Rayleigh and Rice Distributions

Let μ_1, μ_2 be two normally distributed random variables with zero mean and variance σ_0^2 : $\mu_1, \mu_2 \sim N(0, \sigma_0^2)$. A random variable R_1 , defined as $R_1 = \sqrt{\mu_1^2 + \mu_2^2}$ has the probability density function:

$$p_{R_1}(r) = \begin{cases} \frac{r}{\sigma_0^2} \exp\left(-\frac{r^2}{2\sigma_0^2}\right), & r \geq 0 \\ 0, & r < 0 \end{cases}$$

and is said to be *Rayleigh distributed*.

Defining a random variable R_2 as $R_2 = \sqrt{(\mu_1 + a)^2 + \mu_2^2}$, $a \in \Re$ results in the probability density function:

$$p_{R_2}(r) = \begin{cases} \frac{r}{\sigma_0^2} \exp\left(-\frac{r^2 + a^2}{2\sigma_0^2}\right) I_0\left(\frac{ra}{\sigma_0^2}\right), & r \geq 0 \\ 0, & r < 0 \end{cases}$$

where I_0 is the modified Bessel function of the first kind and zero order. R_2 is said to be *Rice distributed*.

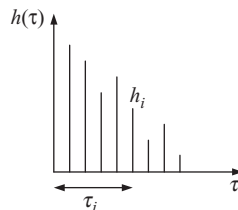


Figure 1.12 Impulse response of a delay-dispersive propagation channel

1.4.2 Maximum Doppler Frequency Shift

In the following, the maximum frequency shift of the received signal experienced by a moving receiver due to the Doppler effect is denoted as f_D , and can be obtained from:

$$f_D = \frac{|\vec{v}|}{c} f_c \quad (1.2)$$

where \vec{v} is the receiver velocity (a stationary transmitter is assumed), c is the speed of light, and f_c is the carrier frequency of the signal. Of course, different frequency components in wideband signals experience different Doppler shifts, which causes some spreading of the signal bandwidth, but this difference is considered small enough to be neglected, as the ratio between the signal bandwidth and carrier frequency is typically small.

The maximum Doppler shift given by (1.2) is an absolute value that corresponds to situations where the receiver is moving radially towards (corresponding to a Doppler shift of $+f_D$) or away from the transmitter (corresponding to $-f_D$). The Doppler shift corresponding to other directions of movement can be obtained as:

$$f_{D,\alpha} = f_D \cos \alpha$$

where α is the angle between directions of the receiver velocity and the arriving signal.

1.4.3 Wide-Sense Stationary Stochastic Processes

A stochastic process is a family of random variables $\{X_t\}_{t \in T}$, where T can be any set. If $T = \mathbb{N}$, the stochastic process is simply a sequence of random variables X_n . Such a sequence is called *strict-sense stationary* if and only if for any $n = 0, 1, \dots$, and any $k = 1, 2, \dots$, (X_0, \dots, X_n) and (X_k, \dots, X_{k+n}) have the same distribution. [10]

A stochastic process is said to be *wide-sense stationary (WSS)* if the mean and autocorrelation of the random variables X_n are invariant to a shift of the origin. More specifically, for any $n = 0, 1, \dots$, $k = 0, 1, \dots$, $E[X_n]$ has a constant value and:

$$E[X_n^* X_k] = r_{XX}(|n - k|)$$

where the asterisk denotes complex conjugation and $r_{XX}(\tau)$ is an autocorrelation function whose value depends only on the time shift τ [16]. Wide-sense stationarity is a weaker condition than strict-sense stationarity, that is, every strict-sense stationary process is wide-sense stationarity, but not vice versa.

For the small-scale fading models described in the following, it is assumed that signals propagate to the receiver antenna along a horizontal plane. Furthermore, it is assumed that the angles of arrival of electromagnetic waves at the receiver antenna are uniformly distributed and that the receiver antenna has a circular-symmetric radiation pattern. As mentioned before, the transmitter antenna is assumed to be stationary, while the receiver moves with velocity \vec{v} .

1.4.4 Rayleigh and Rice Models for Frequency-Nonselective Fading

If the propagation delay differences of the reflected and scattered signal components at the receiver are negligible compared to the symbol interval of the transmission, the channel impulse response can in practice be approximated by a single delta function multiplied by a random variable that describes the amplitude fading. Thus there will be no significant interference caused by overlapping successive transmitted symbols at the receiver, or intersymbol interference, ISI. Also, the channel affects all frequency components of the signal similarly, and the term *frequency-nonselective fading* can be used. In

this case, the small-scale fading is wholly characterized by the distribution and time-variant behaviour of the channel coefficient random variable.

In non-line-of-sight (NLOS) conditions, where there is no direct, unobstructed propagation path from the transmitter to the receiver, both the in-phase and quadrature parts of the received signal are assumed to consist of sums of large numbers of independently faded scattered components. Thus, by the central limit theorem, the fading of the in-phase and quadrature – or real and imaginary – components of the signal can be approximated as independent normally distributed random variables. As described above, this leads to a Rayleigh distribution for the amplitude of the complex fading coefficient. The phase for the complex fading is uniformly distributed between 0 and 2π .

In line-of-sight (LOS) conditions, the received signal can be characterized as a sum of Rayleigh faded NLOS components as described above, and a coherent LOS component with relatively constant power determined by the medium-scale fading. This can be approximated by adding a constant representing the amplitude of the line-of-sight signal contribution to the real part of the complex fading coefficient, which leads to a Rice distribution for the fading amplitude.

As small-scale fading is a function of the receiver location, it is clear that the rate of variation of the fading in time is dependent on the speed of the receiver. Analytically, the receiver velocity determines the Doppler frequency shift of the received signal as given in Section 1.2.3. Based on the maximum Doppler frequency and the angular probability distribution of the received signal components the probability density function of the Doppler frequencies can be calculated. This probability density function is directly proportional to the Doppler power spectral density of the received in-phase and quadrature signal components, the inverse Fourier transform of which gives the autocorrelation function of the channel fading coefficient [16]. It should also be noted that the primary detrimental effect of the Doppler shift in a wireless channel is due to the random directions of arrival of the reflected signal components arriving at the receiver. This randomness means that the received signals are randomly Doppler shifted between $-f_D$ and f_D , which causes a nontrivial broadening of the signal spectrum, and corresponding interference between signal components adjacent in the frequency domain.

Given the assumptions specified in Section 1.2.3, for the NLOS case the Doppler power spectral distribution is completely determined by the maximum Doppler frequency shift given by (1.2), and follows the so called *Jakes power spectral density*, or *Clarke power spectral density*. The LOS case differs from the above in that the Doppler power spectrum also contains a component corresponding to the power and Doppler shift of the line-of-sight signal component. Figure 1.13 illustrates the probability density function of the Doppler shifts and the corresponding autocorrelation function for the Rayleigh fading process. The autocorrelation function can be written as given in [16]:

$$r_{XX}(\tau) = 2\sigma_0^2 J_0(2\pi f_D \tau)$$

where $J_0(\cdot)$ is the zeroth-order Bessel function of the first kind. The *coherence time* T_C of the fading process can be defined as the time interval that fulfills $|r_{XX}(T_C)| = 0.5 r_{XX}(0)$, that is, the time interval after which the value of the autocorrelation has decreased to half of the value at the origin. For the above, $J_0(2\pi f_D \tau) \approx 0.5 \Leftrightarrow 2\pi f_D \tau \approx 1.52$. Thus $T_C \approx 1.52/(2\pi f_D)$. It should however be noted that the coefficient 0.5 assumed above is in no way unique, and also other values for the coherence time could be assigned. However, regardless of the numerical definition, it is important to note that the coherence time is reciprocally proportional to the maximum Doppler frequency f_D .

In practice, the time-variant channel coefficient for small-scale frequency-nonselective fading can be generated by drawing two sequences of normally distributed random numbers – or white Gaussian noise – corresponding to the components of the desired Rayleigh or Rice fading. One way to obtain the correct autocorrelation for the fading is then to low pass filter both of these sequences of random numbers according to the Jakes Doppler spectrum, producing coloured Gaussian noise. Using the filtered sequences as the real and imaginary components of the complex fading coefficient results in approximately the desired probability distribution and autocorrelation described above. Non-ideality

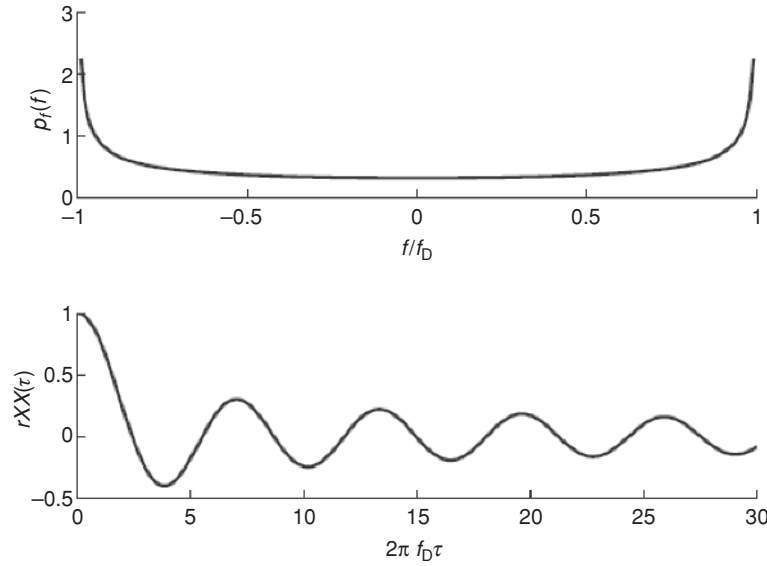


Figure 1.13 Probability density function for Doppler frequency shifts corresponding to the Jakes power spectral density (upper plot), and the corresponding autocorrelation function (lower plot)

arises with this approach mainly from the fact that neither white Gaussian noise nor ideal filters can be realized exactly.

In modelling small-scale fading as described above, the mean and autocorrelation function are typically kept constant, which means that the fading process is wide-sense stationary as defined in Section 1.4.3. It is clear that the mean value of the small-scale fading is dependent on medium- and large-scale fading processes, and thus the assumption of wide-sense stationarity is not generally valid. However, it has been empirically found that small-scale fading can be approximated as a WSS process for short distances (of order tens of wavelengths).

1.4.5 SNR in Rayleigh Fading Channels

In fading channels, the average power of the received signal should be considered a random variable as specified above. Thus, denoting for example the instantaneous signal-to-noise ratio for a Rayleigh channel by random variable Λ_R , the SNR can be written as:

$$\Lambda_R = \frac{\bar{P}_S R^2}{\bar{P}_N}$$

where R is the Rayleigh distributed channel coefficient amplitude. The average SNR, denoted by ρ , is obtained as:

$$\rho = \frac{E[R^2] \bar{P}_S}{\bar{P}_N} = \frac{2\sigma_0^2 \bar{P}_S}{\bar{P}_N}$$

where σ_0 is the variance of the Gaussian components used to define the Rayleigh distribution in Section 1.2.3. In simulations, the average power conveyed by a Rayleigh channel can thus be normalized by selecting $\sigma_0 = 1/\sqrt{2}$. The probability distribution function of Λ_R is obtained as presented for example

in reference [9], and can be written as:

$$p_{\Lambda}(\lambda_R) = \frac{1}{\rho} \exp\left(\frac{-\lambda_R}{\rho}\right), \quad \lambda_R > 0$$

1.5 WSSUS Models for Frequency-Selective Fading

1.5.1 Basic Principles

If the range of propagation delay times from the transmitter to the receiver is not negligible compared to the symbol duration of the transmitted signal, additional distortions of the received signal, such as intersymbol interference and frequency-selective fading, are introduced. In such cases, the frequency-nonselective fading models described above are not generally sufficient to describe the channel.

Adhering to the assumptions given in the previous section, a physical basis for modelling a frequency-selective channel can be found in the ellipses model illustrated for example in [9] and [16]. In this simplified representation of the scattering environment the transmitter and receiver are thought to be at the focal points of elliptical scattering zones, where each ellipse – or set of points with a fixed value for the sum of distances to the transmitter and receiver – defines the geometries of all propagation paths corresponding to a given propagation delay value. This principle is illustrated in Figure 1.14. Thus it is possible to consider the signal components corresponding to each discrete delay value as sums of large numbers of scattered signals with uniform distributions for the angle of arrival at the receiver. This in turn makes it possible to determine the time-variant fading coefficient for each discrete delay value as specified in the previous subsection for frequency-nonselective fading.

Frequency-selective channel models are typically implemented as FIR filters with time-variant complex coefficients by selecting N_i fixed discrete delay values corresponding to the nonzero filter coefficients. The average power for each of the N_i delayed signal components is selected according to a specific *power-delay profile (PDP)*. Given the average powers of each of the nonzero components of the FIR filter, the time-variant complex values for the filter coefficients are generated as WSS fading processes, as described in the previous section. The N_i discrete scattering components of the channel are typically defined as being statistically uncorrelated, which leads to the denomination wide-sense stationary uncorrelated scattering, or WSSUS, models.

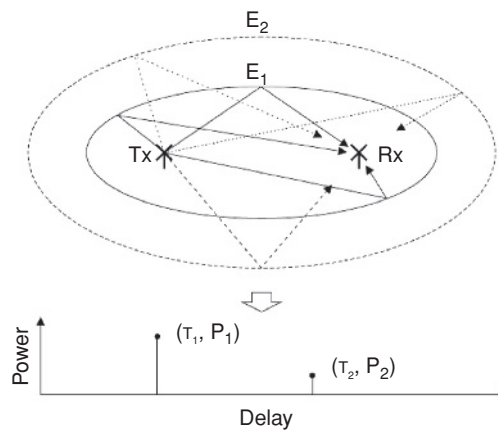


Figure 1.14 Elliptical scattering zones and a corresponding power delay profile

The parameters that characterize a WSSUS channel model according to a given transmission scenario are the PDP, the number and delays of the discrete filter coefficients, or taps, and the types of fading processes and Doppler spectra applied for the individual taps. Typically the continuous-time power delay profile is selected according to an exponential decrease of received signal power as a function of the propagation delay, although sometimes also mixtures of exponential distributions are used. Furthermore, the tap amplitudes are most commonly modelled as Rayleigh fading processes, with possibly a short-delay component defined as line-of-sight, and thus Rice distributed. The Doppler spectra for the independent tap fading processes are typically assumed to have the Jakes distribution, although for long-delay components, or far echoes, Gaussian power spectral densities have been found more accurate in some cases.

1.5.2 Definitions

For a channel with a continuous exponential power delay profile of the form $S(\tau) = (1/\alpha) \exp(-\tau/\alpha)$, $\tau > 0, \alpha > 0$, the mean delay is obtained as $\bar{\tau} = \alpha$ and the *delay spread* S_D as the square root of the second moment $S_D^2 = \alpha^2$. The Fourier transform of $S(\tau)$ is:

$$\psi(f) = \frac{1/\alpha}{1/\alpha + j2\pi f}$$

which gives a measure of the correlation of the fading for a frequency separation of f Hz. The *coherence bandwidth* B_C can be defined – similarly to the coherence time T_C considered previously – as the frequency interval that fulfils $|\psi(B_C)| = 0.5 \psi(0)$, which is obtained by writing $\sqrt{(1/\alpha)^2 + (2\pi B_C)^2} = 2/\alpha$, and results in:

$$B_C = \frac{\sqrt{3}}{2\pi S_D}$$

Again, regardless of the numerical definition it is clear that the coherence bandwidth is reciprocally proportional to the delay spread of an exponential-PDP WSSUS channel. It is also evident that a continuous exponential distribution is characterized by the single free parameter α , which can be selected according to a given delay spread S_D or coherence bandwidth B_C . After defining the continuous distribution, it still remains to determine a discrete power-delay profile that sufficiently describes the selected distribution.

A discrete power-delay profile consists of sets of propagation delay values τ_i , and average scattered signal powers $P_i, i = 1, \dots, N_i$. In the discrete case, the delay spread can be written as:

$$S_D = \sqrt{\frac{1}{P_T} \sum_{i=1}^{N_i} P_i \tau_i^2 - \left(\frac{1}{P_T} \sum_{i=1}^{N_i} P_i \tau_i \right)^2}$$

where P_T is the total power conveyed by the channel, given by $P_T = \sum_{i=1}^{N_i} P_i$. Unless more specific information on the propagation scenario to be modelled is available, it is reasonable to assume that the delay times between consecutive nonzero components in the discrete PDP follow an exponential distribution. This means that the number of channel components within a given delay range follows a Poisson distribution, and those components are uniformly distributed within the given delay range.

References

- [1] M. C. Jeruchim, P. Balaban, K. S. Shanmugan, *Simulation of Communication Systems*, 2nd edition, Kluwer Academic, New York, 2000.
- [2] J. G. Proakis, *Digital Communications*, 3rd edition, McGraw-Hill, 1995.
- [3] R. E. Ziemer, R. W. Peterson, *Introduction to Digital Communication*, Prentice Hall, 2001.

- [4] S. Haykin, *Communication Systems*, John Wiley & Sons, Ltd., 2001.
- [5] T. K. Moon, *Error Correction Coding – Mathematical Methods and Algorithms*, John Wiley & Sons, Ltd., 2005.
- [6] Y. Q. Shi, X. M. Zhang, Z.-C. Ni, N. Ansari, "Interleaving for combating bursts of errors," *IEEE Circuits and Systems Magazine*, vol. 4, First Quarter 2004, 29–42.
- [7] C. Oestges, B. Clerckx, *MIMO Wireless Communications: From Real-World Propagation to Space-Time Code Design*, Elsevier, 2007.
- [8] E. Lutz, D. Cygan, M. Dippold, F. Dolainsky, W. Papke, "The Land Mobile Satellite Communication Channel – Recording, Statistics and Channel Model," *IEEE Trans. Veh. Technol.*, vol. 40, May 1991, 375–386.
- [9] S. R. Saunders, A. Aragón-Zavala, *Antennas and Propagation for Wireless Communication Systems*, 2nd edition, John Wiley & Sons, Ltd., Chichester, 2007.
- [10] R. B. Ash, C. A. Doléans-Dade, *Probability & Measure Theory, Second Edition*, Academic Press, San Diego, 2000.
- [11] N. Blaunstein, J. B. Andersen, *Multipath Phenomena in Cellular Networks*, Artech House, Boston, 2002.
- [12] B. Sklar, "Rayleigh Fading Channels in Mobile Digital Communication Systems Part I: Characterization," *IEEE Communications Magazine*, September 1997, 136–146.
- [13] Y. Okumura, E. Ohmori, K. Fukuda, "Field Strength and its Variability in VHF and UHF Land Mobile Radio Service," *Rev. Elec. Commun. Lab.*, vol. 16, 1968, 825–873.
- [14] M. Hata, "Empirical Formulae for Propagation Loss in Land Mobile Radio Services," *IEEE Trans. Veh. Technol.*, vol. VT-29, 1980, 317–325.
- [15] COST 231, "Urban Transmission Loss Models for Mobile Radio in the 900 MHz and 1800 MHz Bands (rev. 2)," COST 231 TD(90), 119 Rev. 2, Den Haag, 1991.
- [16] M. Pätzold, *Mobile Fading Channels*, John Wiley & Sons, Ltd., Chichester, 2002.
- [17] M. R. Spiegel, *Mathematical Handbook of Formulas and Tables*, McGraw-Hill, Inc., New York, 1994.
- [18] T. J. Wang, J. G. Proakis, E. Masry, J. R. Zeidler, "Performance Degradation of OFDM Systems Due to Doppler Spreading," *IEEE Trans. Wireless Comm.*, vol. 5, June 2006, 1422–1432.
- [19] A. Goldsmith, *Wireless Communications*, Cambridge University Press, New York, 2005.
- [20] M. Gudmunson, "Correlation Model for Shadow Fading in Mobile Radio Systems," *Electronic Letters*, vol. 37, no. 23, pp. 2145–2146, Nov. 1991.
- [21] A. Burr. The multipath problem: an overview. In *IEE Colloquium on Multipath Countermeasures*. London, 23 May 1996, Colloquium Digest 1996/120.
- [22] A. Burr. *Modulation and Coding for Wireless Communication*. Prentice Hall, 2001.
- [23] P. Bello. Characterization of randomly time-variant linear channels. *IEEE Transactions on Communication Systems*, CS-11; 36–393, 1963.